

ISCL: Interdependent Self-Cooperative Learning for Unpaired Image Denoising

Kanggeun Lee and Won-Ki Jeong

Abstract—With the advent of advances in self-supervised learning, paired clean-noisy data are no longer required in deep learning-based image denoising. However, existing blind denoising methods still require the assumption with regard to noise characteristics, such as zero-mean noise distribution and pixel-wise noise-signal independence; this hinders wide adaptation of the method in the medical domain. On the other hand, unpaired learning can overcome limitations related to the assumption on noise characteristics, which makes it more feasible for collecting the training data in real-world scenarios. In this paper, we propose a novel image denoising scheme, Interdependent Self-Cooperative Learning (ISCL), that leverages unpaired learning by combining cyclic adversarial learning with self-supervised residual learning. Unlike the existing unpaired image denoising methods relying on matching data distributions in different domains, the two architectures in ISCL, designed for different tasks, complement each other and boost the learning process. To assess the performance of the proposed method, we conducted extensive experiments in various biomedical image degradation scenarios, such as noise caused by physical characteristics of electron microscopy (EM) devices (film and charging noise), and structural noise found in low-dose computer tomography (CT). We demonstrate that the image quality of our method is superior to conventional and current state-of-the-art deep learning-based image denoising methods, including supervised learning.

Index Terms—Adversarial learning, cooperative learning, cyclic constraint, deep learning, denoising, self-supervision, residual learning.

I. INTRODUCTION

DENOISING is the low-level signal processing technique used to remove specific noise from noisy observation in order to improve the quality of signal analysis. Before deep learning gained its popularity, most image denoising research focused on leveraging image prior information, such as through non-local self-similarity [1], [6], [7], sparsity feature [8]–[11], and total variation [12]–[14]. In recent years, supervised learning methods using deep convolutional neural networks (CNNs) have surpassed the performance of prior-based denoising methods [3], [15]. CNN models can learn to restore a clean target via paired training data without prior knowledge of image or noise. However, their performance is demonstrated only on well-known noise models. The main reason for this is that the training data (clean and noisy image pairs) are generated by adding noise for a given distribution to clean images. Therefore, unconventional image degradation cannot be easily modeled, which makes the application of supervised learning difficult.

Kanggeun Lee is with the school of Electrical and Computer Engineering, UNIST, South Korea (e-mail: leekanggeun@gmail.com).

Won-Ki Jeong is with the Department of Computer Science and Engineering, Korea University, South Korea (e-mail: wkjeong@korea.ac.kr).

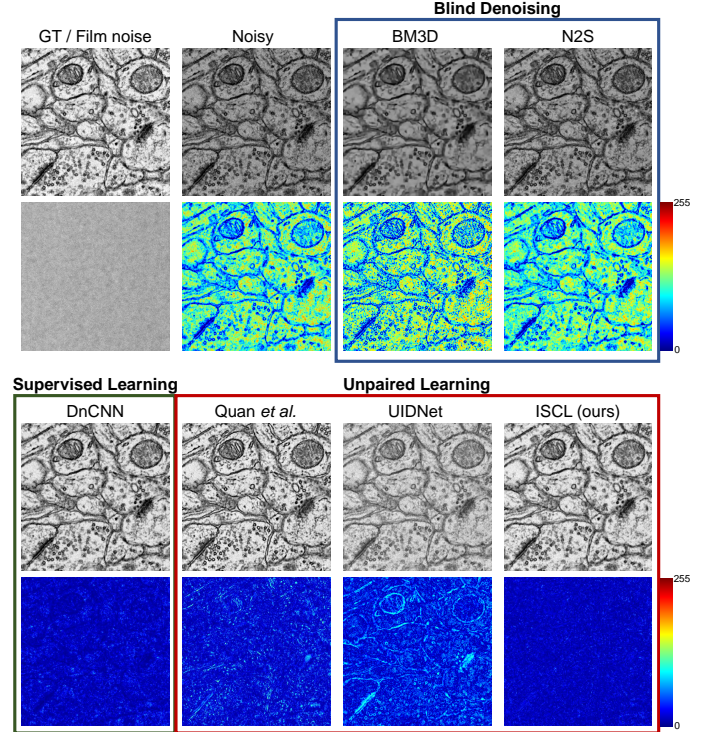


Fig. 1. An example of film noise removal in electron microscopy images. Top left: clean ground-truth image (top) and real film noise image (bottom). BM3D [1] and N2S [2] are blind denoising methods. DnCNN [3] is a supervised learning based denoising method. Quan *et al.* [4], UIDNet [5], and our method (ISCL) are unpaired learning based approaches. Note that ISCL produces lower error than does DnCNN.

Recently, several self-supervised blind denoising methods [2], [16], [17] have shown promising results without the noise prior and the clean-noisy paired training data. The blind spot based approaches predict the clean pixel from the neighbor information of the target pixel based on the self-supervision training. However, these blind denoising methods require zero-mean noise distribution to apply the self-supervision loss. We observed that the state-of-the-art blind denoising and prior-based denoising methods tend to introduce incorrect brightness shifting for non-zero mean noise cases, as shown in Fig. 1 (see BM3D and N2S results are still darker than the ground truth). In addition, noise should be pixel-wise independent under the given noisy observation to employ a blind spot scheme; this is not satisfied in unconventional noise observed in biomedical images. For example, recent high-throughput automatic imaging using transmitted electron microscopy (TEM) [18]–[20] uses electron-lucent

support films, which introduce spatially inhomogeneous noise (i.e., film noise). In addition, prolonged exposure of electron beams onto the thin tissue section causes blob-like damage (i.e., charging noise) in scanning electron microscopy (SEM) images. Such imaging artifacts do not satisfy the necessary conditions for blind denoising.

The primary motivation behind our proposed work stems from the recent advances in unpaired image denoising [4], [5]. Quan *et al.* [4] demonstrated superior denoising performance on electron microscopy (EM) images without paired training data by leveraging three-way cyclic constraints with adversarial training. However, this method requires real noise pattern images (e.g., taking an empty film image, etc.), which is not always feasible in a real scenario (such as low-dose CT (LDCT)). More recently, UIDNet [5] proposed an end-to-end denoising network trained by clean-pseudo noisy pair images where pseudo noisy images are automatically generated via a generative model. However, they only used a simple (weak) generative model to learn the noise distribution from examples, which is insufficient for unconventional noise, as in EM images (see Fig. 1). Our proposed method addresses the above problems via *cooperative learning* – multiple inter-domain mapping functions are trained together in a cooperative manner, which serves as stronger constraints in unsupervised training.

In this paper, we propose a novel image denoising framework, Interdependent Self-Cooperative Learning (ISCL), to restore the clean target from the noise-corrupted image without using either paired supervision or prior knowledge of noise distribution. ISCL consists of two components, CycleGAN [21]-based denoiser learning, and pseudo-label based residual learning of a noise extractor, to boost the performance self-interdependently via cooperative learning. For training the denoiser with the proposed constraints, the noise extractor will assist the learning of the denoiser under the proposed loss. Conversely, the noise extractor will be trained by pairs of pseudo-clean and noisy with the noise consistency. The main contributions of our work can be summarized as follows:

- 1) We propose ISCL, an unpaired image denoiser based on a novel mutually adaptive training that integrates two different tasks. ISCL shows better denoising performance with faster convergence.
- 2) The proposed novel loss functions (i.e., bypass-consistency, discriminator boosting, and noise-consistency) promote the convergence toward an ideal denoiser.
- 3) We propose the novel network architecture and model generalization methods (e.g., stochastic weight averaging (SWA) and lookahead training schemes) suitable for ISCL.
- 4) We demonstrate that the proposed ISCL-based denoiser outperforms state-of-the-art denoising methods, including supervised learning, in the medical domain. We no longer need clean-noisy paired training data to achieve the performance of a supervised denoiser.

II. RELATED WORK

A. Conventional Neural Network Denoising

Despite prior-based denoising had been widely used for many years, deep neural network has become popular in denoising tasks these days due to its superior performance. An earlier work by Jain *et al.* [22] introduced a CNN model for image denoising, and showed the representation powers through the visualization of hidden layers. Burger *et al.* [23] proposed the multi-layer perceptron (MLP) model for denoising; however, it achieved similar or slightly better performance than BM3D over Gaussian noise. More recently, supervised learning of deep CNNs [3], [24], [25] has shown superior performance over conventional image prior based approaches. In particular, DnCNN [3] discovered that the combination of residual learning [26] and batch normalization [27] can greatly assist the training of CNNs for speeding up the training and boosting the denoising performance; however, it has a limitation with regard to the presence of noisy-residual (i.e., noise image) pairs. Recently, Lehtinen *et al.* [28] introduced a Noise2Noise (N2N) method that can achieve similar performance employing only noisy pairs to the supervised learning performance. Even though N2N can overcome the requirement of clean-noisy pairs in the supervised learning, noise statistics is still an essential condition to generate noisy-noisy pairs.

B. Blind Denoising

Blind denoising aims to restore noisy observations that are corrupted by unknown noise distribution without the supervision of clean targets. Deep Image Prior (DIP) [29] showed the usability of a hand-crafted prior, generated by a random-initialized neural network, for the image denoising task. The internal image prior based approach is the early method of blind denoising. Recently, self-supervised learning based blind denoising approaches achieved the performance closed to that of supervised learning. N2S [2] and N2V [16] proposed a blind-spot scheme for training a CNN denoiser with only noisy images. Furthermore, they achieved significantly reduced deploying time through the external image prior. Blind denoising methods do not require clean-noisy pairs, but they still rely on the assumption of noise characteristics, such as zero-mean noise and pixel-wise signal-noise independence. More recently, S2S [17] successfully showed superior performance using internal image prior, that is, Bernoulli-sampled instances of only a single noisy image. Even though S2S is trained using a single noisy image, S2S outperforms external image prior based blind denoising methods.

C. Unpaired Image Denoising

To overcome the limitation of the blind denoising methods, unpaired image denoising methods [4], [30]–[32] have gained much attention these days as a new denoising approach. Since the unpaired image denoising approaches can leverage the supervision of clean targets, zero-mean noise and pixel-wise signal independent assumptions are not prerequisite anymore. Furthermore, collecting of unpaired data is more feasible in a real setup, compared to using clean-noisy

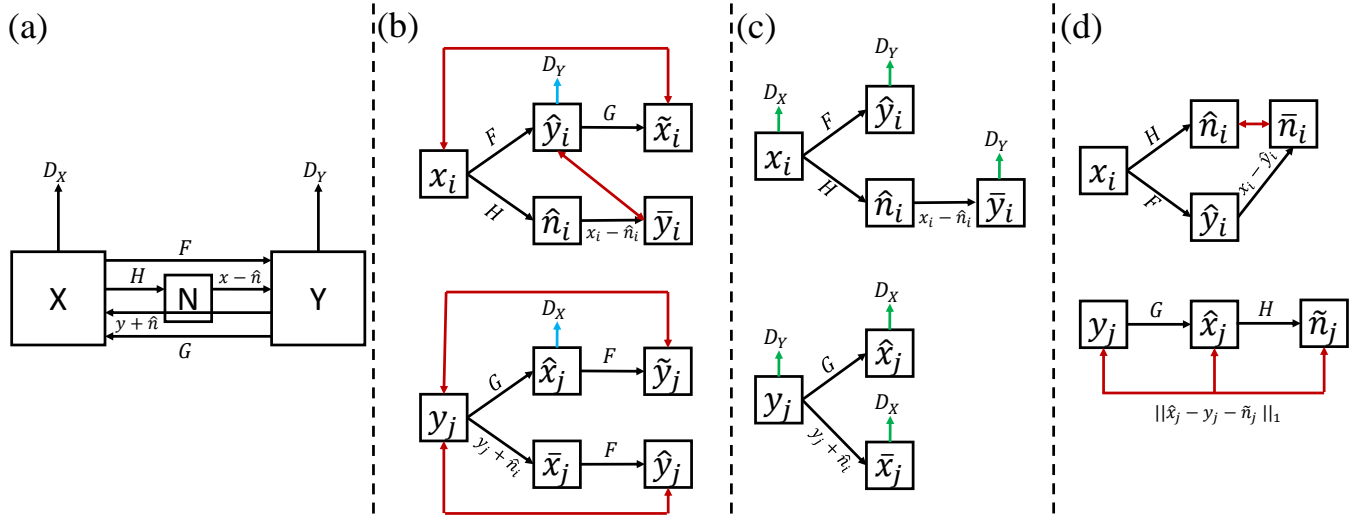


Fig. 2. (a) Flow graph of ISCL. Our proposed scheme has three mapping functions, $F : X \rightarrow Y$, $G : Y \rightarrow X$, and $H : X \rightarrow N$ with two discriminators, D_X and D_Y . X , Y , and N are domains of noisy target, clean source, and noise of noisy target, respectively. (b) Training process of two mapping functions, F and G . The blue means that the F and G are encouraged by outputs of D_X and D_Y for translation from one domain to the other as in adversarial learning. The red indicates the mean absolute error (MAE) between two instances as a cycle consistency. (c) Training process of two discriminators, D_X and D_Y . Each discriminator can learn to distinguish between real and fake generated by F , G and H . The green indicates the inputs for the learning of each discriminator. (d) Training process of the mapping function H . The H can be learned from pseudo-noise label \tilde{n}_i . Furthermore, the other constraint is to restrict the difference between pseudo-noise $\hat{x}_j - y_j$ and the output noise $H(\hat{x}_j)$.

pairs. GCBD [30] demonstrated that the generative adversarial network (GAN) [33] can be trained to estimate the noise distribution from the noisy observations. However, it has a critical limitation: a zero-mean noise assumption. Quan *et al.* [4] proposed an asymmetrically cyclic adversarial network that consists of two generators. One generator can decompose a noisy observation to a clean-noise pair. The purpose of the other generator is to combine the clean-noise pair as a pseudo noisy image. The combination of two generators as an asymmetrical CycleGAN outperformed the state-of-the-art blind denoising methods without any image prior assumptions. However, it still has a limitation of requiring real noise image, which is often difficult to acquire. UIDNet [5] employed a conditional GAN (cGAN) to learn the noise distribution from noisy observations and generated clean-pseudo noisy pairs to train a denoiser. To secure the stability of training, they used the WGAN-GP [34] loss, that is, an improved version of WGAN [35] with a gradient penalty. Furthermore, they proposed a sharpening technique that boosts the performance of the discriminator through the concatenation of input and filtered input. However, as shown in the following sections, using a simple generative model to learn the noise distribution from examples is the main weakness of the method.

III. METHOD

In this section, we introduce the details of ISCL. We focus on mapping between the noisy image domain X and the clean image domain Y using the two inter-domain mapping functions F and G . Here, F serves as a denoiser, and G is the inverse of F , which is a noise generator (i.e., adding noise to the given clean image). To train F and G , we employ D_X and D_Y , which are discriminators, to distinguish a real sample and a fake sample (i.e., a domain shifted sample

from another domain). However, adversarial losses are not sufficient constraints to train the discriminators for translating an ideal clean sample y_i from a noisy sample x_i due to the wide possible mapping space of $F(x_i)$. To generate a tighter mapping space from x_i , CycleGAN [21] proposed cycle consistency, i.e., $x \approx G(F(x))$ and $y \approx F(G(y))$, where $x \sim \mathcal{X}$ and $y \sim \mathcal{Y}$; \mathcal{X} and \mathcal{Y} are data distributions for the noisy observations and the clean sources, respectively. Therefore, we were faced with the problem that additional constraints are required to optimize F and G into bijective functions, i.e., a function for an ideal denoiser.

Suppose that F and G are bijective functions. Then, we can extract only a single noise image from x_i by subtracting $F(x_i)$ from it. In other words, we can infer that there exists an injective function $H : X \rightarrow N$, where N is a noise domain, that can extract the noise from the noisy observation. Based on this inference, we propose the cooperative learning concept to optimize the CycleGAN model and the noise extractor model simultaneously. In greater detail, five functions (i.e., F , G , D_X , D_Y , and H) will be trained by assisting each other interdependently. We denote the denoiser trained by Interdependent Self-Cooperative Learning “ISCL”.

A. Bypass-Consistency

Here, we introduce the nested cycle consistency consisting of cycle-consistency and bypass-consistency. In Fig. 2b, we can find two mapping functions, F and G , as generative models, trained by the following loss:

$$\begin{aligned} \mathcal{L}_{gen}(F, G, H, D_X, D_Y) = & \mathcal{L}_F(F, D_Y) \\ & + \mathcal{L}_G(G, D_X) \\ & + \lambda \mathcal{L}_{nested}(F, G, H), \end{aligned} \quad (1)$$

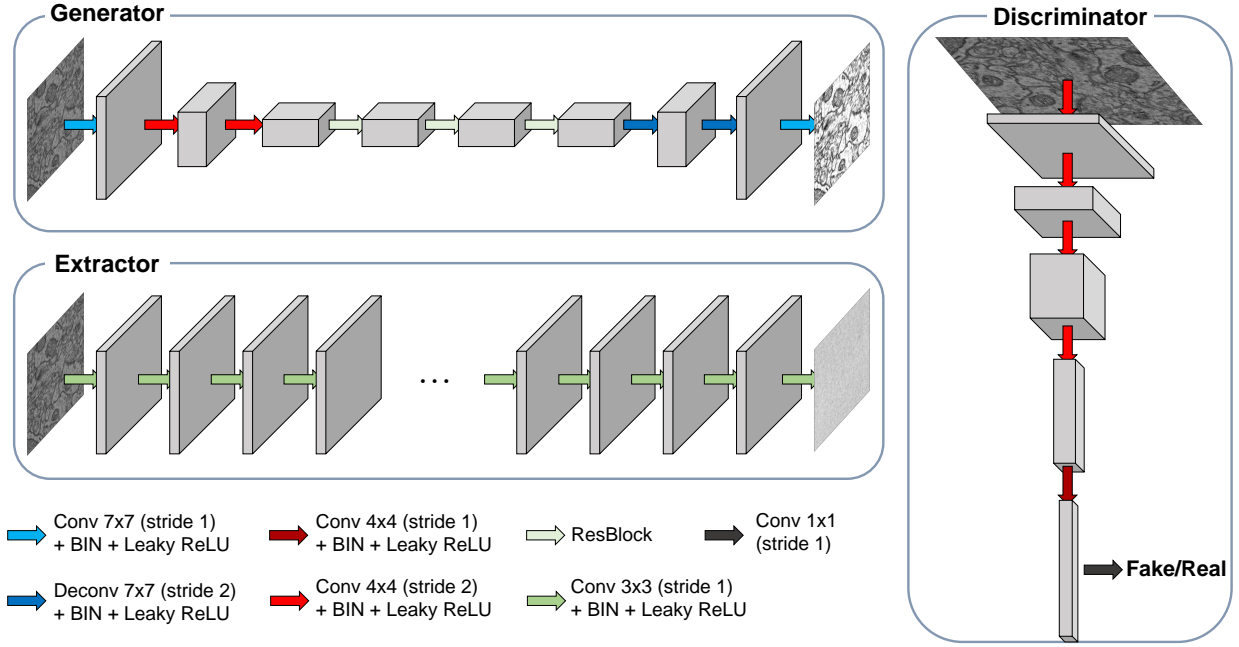


Fig. 3. Network structure: F and G employ generator structure. H is an extractor. D_X and D_Y are discriminators.

where F translates a noisy target domain X to a clean source domain Y under the supervision of D_Y , and vice versa for G and D_X . In detail, we borrow the generative loss based on hinge loss [36] to define \mathcal{L}_F and \mathcal{L}_G as follows:

$$\mathcal{L}_F(F, D_Y) = -\mathbb{E}_{x \sim \mathcal{X}}[D_Y(F(x))] \quad (2)$$

$$\mathcal{L}_G(G, D_X) = -\mathbb{E}_{y \sim \mathcal{Y}}[D_X(G(y))] \quad (3)$$

and the nested cycle-consistency loss is defined as follows:

$$\mathcal{L}_{nested}(F, G, H) = \mathcal{L}_{cycle}(F, G) + \mathcal{L}_{bypass}(F, H). \quad (4)$$

The cycle consistency loss \mathcal{L}_{cycle} restricts the mapping space of $G(F(x))$ and $F(G(y))$, which is defined as follows:

$$\mathcal{L}_{cycle} = \mathbb{E}_{x \sim \mathcal{X}} \|x - G(F(x))\|_1 + \mathbb{E}_{y \sim \mathcal{Y}} \|y - F(G(y))\|_1. \quad (5)$$

Note that, even though the above cycle-consistency loss promotes bijections $F \circ G$ and $G \circ F$, there is no guarantee that both F and G are actually the bijective functions after convergence. In other words, using only cycle-consistency is still insufficient to converge each function into the bijective function. If the injective function H is available, then \bar{y} is a pseudo-clean label for x , as shown in Fig. 2 top. Then, we can restrict the mapping space of $F(x)$ into \bar{y} . Moreover, we adopts the pseudo-noisy \bar{x} to restrict the mapping space of $F(\bar{x})$ into y real sample. Finally, we propose the bypass-consistency to restrict the mapping space of the target denoiser F through the pseudo label generated by H as follows:

$$\mathcal{L}_{bypass}(F, H) = \mathbb{E}_{x \sim \mathcal{X}} \|F(x) - (x - H(x))\|_1 + \mathbb{E}_{x \sim \mathcal{X}, y \sim \mathcal{Y}} \|y - F(y + H(x))\|_1. \quad (6)$$

In other words, there exists two different approaches to mapping a noisy image x into a clean source domain Y , either a bijective function F or an injective function H ,

as shown in Fig. 2b. The bypass-consistency promotes two outputs generated by the two mapping functions F and H to be similar to each other to satisfy our assumption. In addition, as shown in Fig. 2 bottom, the reconstructed outputs \hat{y}_j and \hat{y}_j generated from real clean source y_j through $F(G(y_j))$ and $F(y_j + H(x_i))$ should be similar to the clean source y_j . In summary, we introduced the nested cycle-consistency to cooperate between the generators of CycleGAN and the noise extractor H under the supervision of discriminators D_X and D_Y .

B. Boosting Discriminators

Discriminators use real and fake samples to optimize the model based on the adversarial losses. In conventional adversarial learning, discriminators D_X and D_Y depend on only fake samples generated by F and G . To improve the ability of discriminators, the fake samples generated by H also have the advantage of the cooperative learning. We propose an additional boosting loss to improve the discriminator's capability to distinguish fake samples as follows:

$$\begin{aligned} \mathcal{L}_{dis}(F, G, H, D_X, D_Y) &= \mathcal{L}_{D_Y}(F, D_Y) \\ &\quad + \mathcal{L}_{D_X}(G, D_X) \\ &\quad + \mathcal{L}_{bst}(H, D_X, D_Y). \end{aligned} \quad (7)$$

For the discriminators, we employ hinge loss [36] to train the adversarial network against the generators, F and G as follows:

$$\begin{aligned} \mathcal{L}_{D_Y}(F, D_Y) &= \mathbb{E}_{y \sim \mathcal{Y}} [\min(0, 1 - D_Y(y))] \\ &\quad + \mathbb{E}_{x \sim \mathcal{X}} [\min(0, D_Y(F(x)))] \\ \mathcal{L}_{D_X}(G, D_X) &= \mathbb{E}_{x \sim \mathcal{X}} [\min(0, 1 - D_X(x))] \\ &\quad + \mathbb{E}_{y \sim \mathcal{Y}} [\min(0, D_X(G(y)))] \end{aligned} \quad (8)$$

Algorithm 1: Interdependent Self-Cooperative Learning Algorithm

Require: $\lambda = 30$ for \mathcal{L}_{nested} , $\gamma = 0.5$, N_{epoch} , N_{iter} , batch size m , patch size of 64×64

Require: N_{swa} , cycle length c , synchronization period k , weights step size α

Require: Initialize parameters $\theta^{(F)}$, $\theta^{(G)}$, $\theta^{(H)}$, $\theta^{(D_X)}$, $\theta^{(D_Y)}$

$\phi^{(D_X)} \leftarrow \theta^{(D_X)}$, $\phi^{(D_Y)} \leftarrow \theta^{(D_Y)}$, $\phi^{(H)} \leftarrow \theta^{(H)}$

for $e = 0, \dots, N_{epoch}$ **do**

if $e \geq N_{swa}$ **then**

$\phi^{(F)} \leftarrow \theta^{(F)}$, $\phi^{(G)} \leftarrow \theta^{(G)}$

end

for $t = 1, \dots, N_{iter}$ **do**

 Unpaired mini-batch of noisy image patches $\{x^{(i)}\}_{i=1}^m$, and clean image patches $\{y^{(j)}\}_{j=1}^m$ from data generating distribution \mathcal{X} and \mathcal{Y} feed into each loss.

 Update F, G : $\theta^{(F)}, \theta^{(G)} \leftarrow \text{Radam}$

$(\nabla_{\theta^{(F)}, \theta^{(G)}} \mathcal{L}_{gen}(F, G, H, D_X, D_Y), \theta^{(F)}, \theta^{(G)})$

if $e \geq N_{swa}$ **then**

if $\text{mod}(t + (e - N_{swa}) * N_{iter}, c) = 0$ **then**

$n_{models} \leftarrow \frac{t + (e - N_{swa}) * N_{iter}}{c}$

$\phi^{(F)} \leftarrow \frac{\phi^{(F)} \cdot n_{models} + \theta^{(F)}}{n_{models} + 1}$

$\phi^{(G)} \leftarrow \frac{\phi^{(G)} \cdot n_{models} + \theta^{(G)}}{n_{models} + 1}$

end

end

 Update D_X, D_Y : $\theta^{(D_X)}, \theta^{(D_Y)} \leftarrow \text{Radam}$

$\nabla_{\theta^{(D_X)}, \theta^{(D_Y)}} \mathcal{L}_{dis}(F, G, H, D_X, D_Y), \theta^{(D_X)}, \theta^{(D_Y)})$

 Update H : $\theta^{(H)} \leftarrow \text{Radam}$

$\nabla_{\theta^{(H)}} \mathcal{L}_{self}(F, G, H), \theta^{(H)})$

if $\text{mod}(t + e * N_{iter}, k) = 0$ **then**

$\phi^{(D_X)} \leftarrow \phi^{(D_X)} + \alpha(\theta^{(D_X)} - \phi^{(D_X)})$

$\phi^{(D_Y)} \leftarrow \phi^{(D_Y)} + \alpha(\theta^{(D_Y)} - \phi^{(D_Y)})$

$\phi^{(H)} \leftarrow \phi^{(H)} + \alpha(\theta^{(H)} - \phi^{(H)})$

$\theta^{(D_X)} \leftarrow \phi^{(D_X)}$, $\theta^{(D_Y)} \leftarrow \phi^{(D_Y)}$,

$\theta^{(H)} \leftarrow \phi^{(H)}$

end

end

end

return $\phi^{(F)}, \phi^{(G)}, \phi^{(D_X)}, \phi^{(D_Y)}, \phi^{(H)}$

and the boosting loss is defined with additional fake samples generated by H as follows:

$$\begin{aligned} \mathcal{L}_{bst}(H, D_X, D_Y) = & \mathbb{E}_{x \sim \mathcal{X}}[\min(0, D_Y(x - H(x)))] \\ & + \mathbb{E}_{x \sim \mathcal{X}, y \sim \mathcal{Y}}[\min(0, D_X(y + H(x)))] \end{aligned} \quad (9)$$

\mathcal{L}_{bst} promotes the ability to discriminate fake clean \bar{y} and fake noisy \bar{x} using a noise $H(x)$, as shown in Fig. 2c. The discriminators are interdependently optimized by the outputs of generators and the noise extractor with real unpaired data.

C. Pseudo-Noise Label

The basic concept of self-residual learning is to construct a pseudo-noise label from CycleGAN for training the noise

extractor. In the next step, the noise extractor H will assist the training of CycleGAN to boost the performance. We express the mapping function H as the noise extractor, as shown in Fig. 2d. If F is a bijective function, then we can generate a unique noise map n by $x - F(x)$. In other words, we employ the pseudo-noise label \bar{n} generated by $x - F(x)$ to learn the capability of the noise extraction. Using this pseudo-noise label, we can optimize the mapping function H by the following loss:

$$\mathcal{L}_{pseudo}(F, H) = \mathbb{E}_{x \sim \mathcal{X}} \|H(x) - (x - F(x))\|_1. \quad (10)$$

In addition, we can generate the single noise n by $G(y) - y$ if G is also a bijective function. Moreover, $H(G(y))$ can extract the same noise map n because of the injective function assumption for H . To reduce (constrain) the mapping space of the $H(\hat{x})$, we add the noise-consistency loss as follows:

$$\mathcal{L}_{nc}(G, H) = \mathbb{E}_{y \sim \mathcal{Y}} \|G(y) - y - (H(G(y)) - y)\|_1. \quad (11)$$

Finally, we can optimize H function with the following loss:

$$\mathcal{L}_{self}(F, G, H) = \mathcal{L}_{pseudo}(F, H) + \mathcal{L}_{nc}(G, H). \quad (12)$$

\mathcal{L}_{self} is a self-supervision based loss because it utilizes each sample x or y even if x and y are unpaired. In other words, the self-residual learning through \mathcal{L}_{self} can be applicable to the task in which unpaired data are available. The self-residual learning with \mathcal{L}_{self} leads to stable convergence and performance improvement similar to co-teaching scheme [37]. Algorithm 1 is the pseudo-code of ISCL where stochastic weight averaging (SWA) [38] and Lookahead [39] schemes are used with the RADam [40] optimizer for optimal training. The final denoising output of ISCL is an ensemble of outputs F and H as follows:

$$y = \gamma F(x) + (1 - \gamma)(x - H(x)) \quad (13)$$

where $0 \leq \gamma \leq 1$. We used $\gamma = 0.5$ in our experiments.

IV. EXPERIMENTS

In this section, we demonstrate the performance of ISCL via quantitative and qualitative evaluation on synthetic and real EM datasets and a low-dose CT dataset. For the CT dataset, we also conducted ablation study to elaborate how each loss contributes to the performance of the method. Our experiments consists of three parts: (1) Ablation study and performance assessment on the 2016 NIH-AAPM-Mayo Clinic Low Dose CT Grand Challenge dataset [41]; (2) Quantitative performance evaluation on synthetic noisy EM image generated by adding film noise and charge noise into clean EM images [4]; and (3) Qualitative performance comparison on real EM images corrupted with film noise and charge noise in which the ground-truth clean images are not available [4].

As for comparison with other methods, we used the source code provided by the authors (downloaded from their website). We used the hyper-parameters empirically found for the best performance, or used the best parameters reported by the authors.

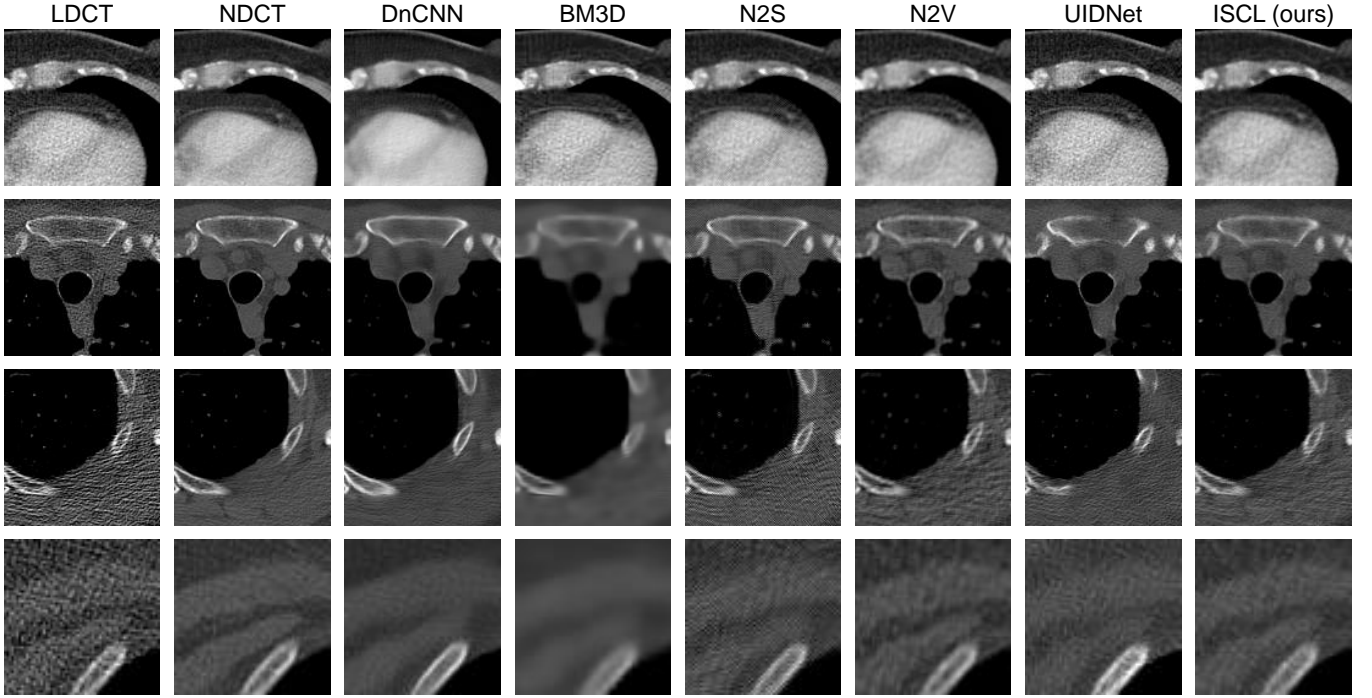


Fig. 4. Qualitative performance of a supervised denoiser (i.e. DnCNN), blind denoisers (i.e. BM3D, N2S, and N2V), and unpaired image denoisers (i.e. UIDNet and ISCL). First row indicates the denoising results of the small portion of abdominal that are normalized under $[-160, 240]$ Hounsfield Unit (HU). The other rows mean that the denoising results of the small portions of chest that are normalized under $[-400, 1000]$ HU.

TABLE I
PERFORMANCE COMPARISON ON LOW-DOSE CT DATASET. P.S.: PAIRED SUPERVISION, B.S.: BLIND SUPERVISION, U.S.: UNPAIRED SUPERVISION, (A) CYCLEGA ONLY, (B) SELF-RESIDUAL NETWORK TRAINED BY PSEUDO-NOISE LABEL, (C) \mathcal{L}_{bypass} , (D) \mathcal{L}_{bst} , (E) \mathcal{L}_{nc} . BOTTOM-MOST RESULTS ARE FINAL PERFORMANCE OF THE PROPOSED METHOD ISCL. THE BEST PSNR IN EACH CASE EXCEPT P.S. IS HIGHLIGHTED IN BOLD.

Type	Method	Abdominal		Chest	
		PSNR	SSIM	PSNR	SSIM
P.S.	DnCNN [3]	30.57	0.8192	27.47	0.7354
B.S.	BM3D [1]	30.31	0.8730	26.75	0.7336
	N2S [2]	28.94	0.8355	23.76	0.6672
	N2V [16]	28.32	0.7961	26.30	0.7283
U.S.	UIDNet [5]	28.91	0.8470	24.15	0.7221
	(A)	22.33	0.7561	22.06	0.6236
	(A)+(B)	22.10	0.7954	22.58	0.5815
	(A)+(B)+(C)	29.43	0.8811	26.61	0.7533
	(A)+(B)+(C)+(D)	30.13	0.8819	26.89	0.7569
	(A)+(B)+(C)+(D)+(E)	30.61	0.8849	26.93	0.7587

A. Implementation Details

We construct five deep neural networks, generators F and G , discriminators D_X and D_Y , and noise extractor H , to train the ISCL denoiser. All architectures are illustrated in Fig. 3. The noise extractor H is adopted from DnCNN [3] except the normalization method. We replace the batch normalization [27] layers with Batch-Instance normalization [42] layers that can have advantages of batch normalization and instance normalization [43]; it preserves useful textures while selec-

tively normalizing only disturbing textures. As shown in Fig. 3, we adopt a fully convolutional network architecture [44] to handle different input sizes. We randomly extract patches of size 64×64 to increase the batch size to fit to the limited GPU memory size. Each mini-batch contains randomly selected patches from unpaired clean and noisy images. As shown in Algorithm 1, the three RAdam [40] optimizers are used to train the generators, the discriminators, and the extractor. Furthermore, since self-cooperative learning is sensitive to each other performance at each iteration, we empirically found the suitable generalization methods for each network architecture. We employ an SWA [38] for generalization of generators to avoid unstable convergence since the unstable performance at each iteration negatively affects the self-cooperative learning. We also employ the Lookahead [39] generalization scheme to improve the learning stability for discriminators D_X and D_Y , and noise extractor H . The learning rate is initially set to $1e-4$, and is linearly decayed up to $1e-6$ for all RAdam optimizers.

B. Low-Dose CT Denoising

For performance evaluation on low-dose CT, we used the abdominal and chest CT images in the 2016 NIH-AAPM-Mayo Clinic Low Dose CT Grand Challenge dataset [41]. In this dataset, LDCT and normal dose CT (NDCT) indicate the noisy and clean images, respectively. We randomly selected 30 anonymous patients for training and 10 anonymous patients for testing in the abdominal and chest datasets. We collected 2944 and 1433 slices (each is of size 512×512 pixels) for training and testing in the abdominal case, respectively. For the chest

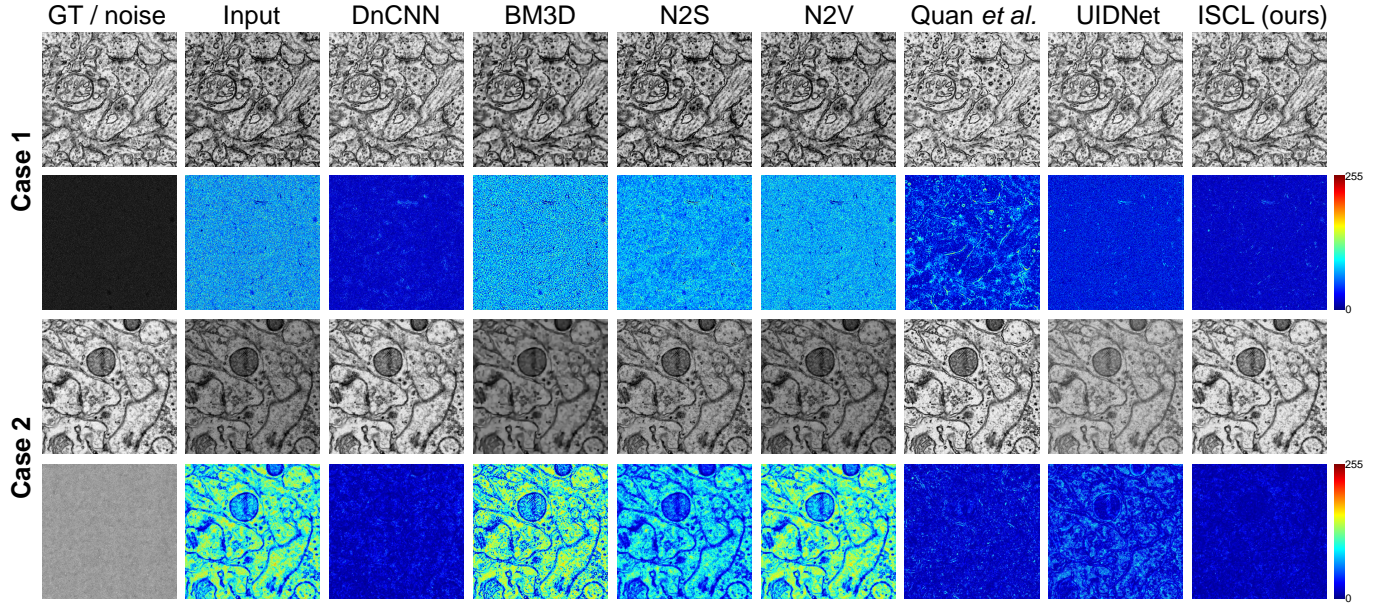


Fig. 5. Comparison results of synthetic noisy data across state-of-the-art methods in case 1 and 2. Second and fourth rows are the error heat map showing the difference between the ground-truth and the result.

case, we randomly selected 3000 slices from among 6687 training images to reduce the training cost, and collected 3254 slices from 10 anonymous patients for testing. We compared ISCL with a supervised denoiser (i.e., DnCNN [3]), blind denoisers (i.e., BM3D [1], N2S [2], and N2V [16]), and an unpaired image denoiser (i.e., UIDNet [5]). For the blind denoising methods, all LDCT slices of the training set are used to train N2S and N2V models without NDCT. Unlike the supervised learning and the blind denoising methods, UIDNet and ISCL require unpaired data. Therefore, we divided the data into two non-overlapping groups; one group contains only NDCT as a clean dataset, the other group contains only LDCT as a noisy dataset. Fig. 4 provides qualitative comparison of the results. BM3D generated overly smoothed results even though it achieved higher PSNR and SSIM than N2S, N2V, and UIDNet. DnCNN and ISCL generated better result although DnCNN results seem more blurrier than those of ISCL. The SSIM values in Table I support these observations. Table I summarizes the quantitative performance assessment of the methods. The proposed method (ISCL) achieved the highest PSNR and SSIM scores compare to the blind denoising methods (i.e., BM3D, N2S, and N2V) and UIDNet along with supervised learning on abdominal CT. Moreover, we also observed that the performance gap between (A)+(B) and (A)+(B)+(C) indicates the effectiveness of \mathcal{L}_{bypass} . We observed that including more losses (\mathcal{L}_{bypass} , \mathcal{L}_{bst} , \mathcal{L}_{nc}) always lead to better performance. We conclude that ISCL achieved performance comparable to DnCNN supervised denoiser without paired training data, which is difficult to acquire in some biomedical applications.

C. Synthetic Noisy EM Denoising

For quantitative assessment, we used synthetically generated noisy EM images. We used the same dataset of charge noise

TABLE II
SPECIFICATIONS FOR OUR EM EXPERIMENT CASES.

Case	Noise-Free Images	Noise Types	Noisy Images (Scenario)
1	TEM_{ZB}	Charge	$TEM_{ZB} + \text{Charge}$ (Synthetic)
2	TEM_{DR5}	Film	$TEM_{DR5} + \text{Film}$ (Synthetic)
3	TEM_{ZB}	Charge	SEM_{ZB} (Real)
4	TEM_{DR5}	Film	TEM_{PPC} (Real)

TABLE III
P.S.: PAIRED SUPERVISION, B.S.: BLIND SUPERVISION, U.S.: UNPAIRED SUPERVISION. QUANTITATIVE PSNR AND SSIM RESULTS ON CASE 1 AND 2. THE BEST PSNR IN EACH CASE EXCEPT P.S. IS HIGHLIGHTED IN BOLD.

Type	Method	Charge noise		Film noise	
		PSNR	SSIM	PSNR	SSIM
P.S.	DnCNN [3]	28.27	0.9172	27.55	0.8964
B.S.	BM3D [1]	17.85	0.7873	12.85	0.6097
	N2S [2]	18.75	0.8680	13.47	0.7942
	N2V [16]	18.06	0.8286	12.86	0.6860
U.S.	Quan <i>et al.</i> [4]	22.32	0.8785	23.44	0.8288
	UIDNet [5]	23.11	0.8592	21.34	0.7826
	ISCL (ours)	27.12	0.9054	27.06	0.8915

and film noise first used in Quan *et al.* [4], as listed in Table II. We used 128 images of 512×512 for each type of noise free (TEM_{ZB} and TEM_{DR5}) and noisy (synthetically generated) images, listed as case 1 and 2. TEM_{ZB} and TEM_{DR5} are noise-free clean TEM images of a juvenile zebrafish brain and a mouse brain respectively, and the corresponding noisy images are synthetically generated by adding a charge noise (for TEM_{ZB}) or multiplying a film noise (for TEM_{DR5}). The example noise images are shown in Fig. 5 (under the ground truth image). To avoid test set selection bias, we ran 4-fold

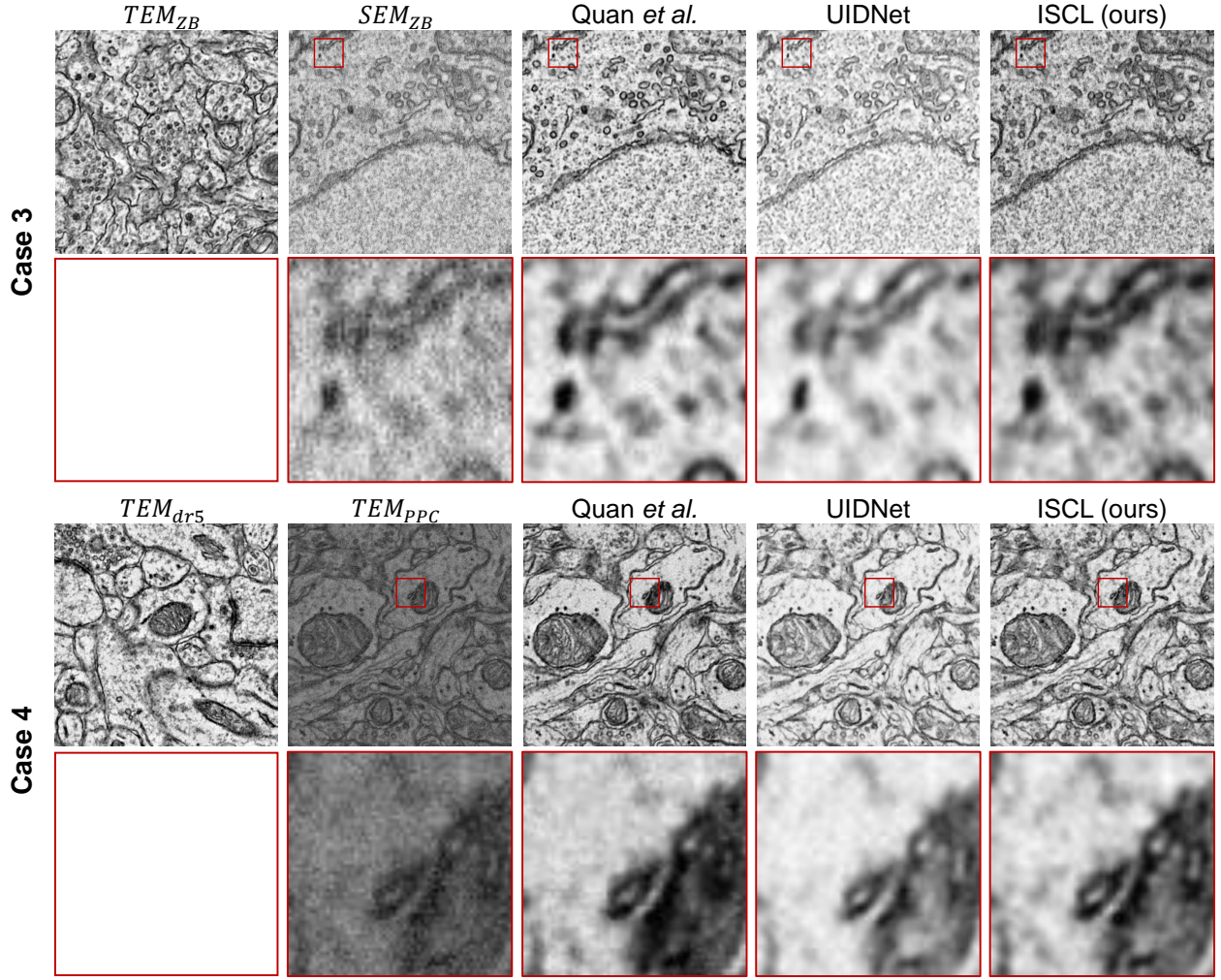


Fig. 6. Qualitative assessment of the denoising quality without using ground truth on real EM images corrupted with charge noise and film noise. Note that the proposed method enhances the quality of the input noisy images comparable to the clean TEM images (shown on the left) without paired clean ground truth images.

cross validation (3 to 1 split) where each test set consists of 32 images. To compensate the small size of EM training set, we applied rotation and mirroring data augmentation. As shown in the first row of Fig. 5, we observed that blind denoising methods fail to recover the correct brightness due to the non-zero mean noise distribution. We also observed in the error heat map of case 1 that the blind denoising methods did not remove structural noise either. PSNR and SSIM values in Table III also confirm this observation. As for unpaired denoising cases, the result of Quan *et al.* on case 1 shows strong errors near the edges. UIDNet also shows Gaussian noise-like corruption in the result of case 1. For case 2, we discovered that the shape dependent noise in the result of UIDNet. Unlike the other unpaired image denoising methods, ISCL successfully restores the structure noise with correct brightness in case 1 and case 2 of Fig. 5. In addition to qualitative results, ISCL outperforms all comparison methods except the supervised learning in Table III. Furthermore, ISCL achieves PSNRs $> 27\text{dB}$ that is the highest values among unpaired denoising methods. Consequently, it is clearly shown that ISCL can effectively eliminate unconventional noise cor-

ruption via training using only unpaired data without noise distribution prior.

D. Real Noisy EM Denoising

To assess the performance of the proposed method in a realistic setup, we compared the denoising quality on SEM_{ZB} (case 3) and TEM_{PPC} (case 4), which are real noisy EM images corrupted with charge noise and film noise, respectively. In this experiment, we used clean EM images (TEM_{ZB} and TEM_{DR5}) as unpaired clean images to train unpaired denoising methods. We already observed in the previous synthetic noise removal experiment that blind denoising methods performed poorly on film and charge noise. Therefore, we tested only unpaired denoising methods in this experiment.

In the absence of ground truth data, we can only assess the visual quality. Fig. 6 shows the qualitative results for case 3 and 4. We observed that Quan *et al.* increases contrast of images and tends to over-emphasize the cell membranes, while UIDNet tends to make images brighter. We also observed that the membranes in UIDNet results are much dimmer and fuzzier compared to Quan *et al.* and ISCL. ISCL restores

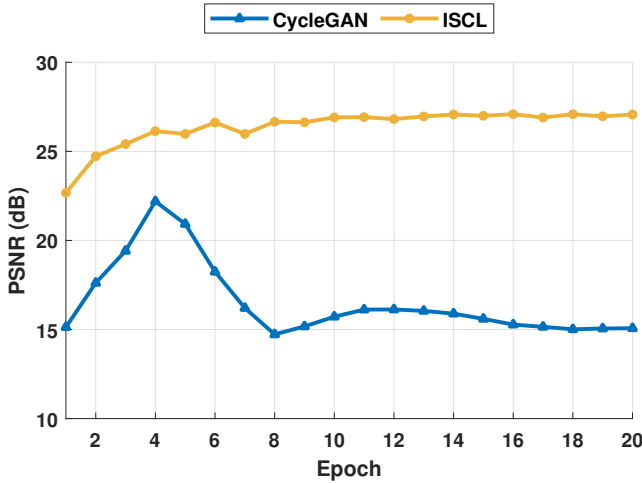


Fig. 7. An example graph for validation data of film noise (case 2); the validation data is also unseen data during training. In this graph, the performance of ISCL indicates the validation PSNR of $F(x)$ instead the ensemble $(F(x) + x - H(x)) * 0.5$ for a fair comparison.

images with a good balance between contrast and sharpness. In summary, ISCL demonstrated similar or better denoising quality compared to Quan *et al.*, while outperforming UIDNet in terms of overall image contrast and feature details.

E. Discussion

In the previous section, we demonstrated how the proposed constraints contribute to the performance of ISCL (Table I). To further analyze the source of the performance of ISCL, we compare the validation performance graph of a vanilla CycleGAN and ISCL (Fig. 7). In this experiment, we used the same generator architecture for both methods; the only difference is that ISCL is trained using the proposed self-cooperative learning scheme. As shown in Fig. 7, the vanilla CycleGAN without the self-cooperative learning showed unstable performance; furthermore, it converged to lower validation performance even though SWA and Lookahead were applied to generators and discriminators. However, ISCL showed stable performance with higher PSNR for the validation data. Moreover, it reached the level of the maximum PSNR of CycleGAN even if each generator F of CycleGAN and ISCL for denoising has the same structure, as shown in Fig. 3. We conclude that self-cooperative learning closely leads to a global optimal point under the same conditions, such as the number of parameters and training data. Despite the performance improvement, the noise extractor is required to utilize our method. This will increase the computation cost and memory requirements. More in-depth efficiency analysis of ISCL is left for the future work.

V. CONCLUSION

In this paper, we introduced a novel denoiser, ISCL, with which the unpaired image denoising becomes feasible. ISCL outperformed the state-of-the-art blind denoising methods (i.e., BM3D, N2S, and N2V) and the unpaired image denoising methods (i.e., Quan *et al.* and UIDNet). Furthermore, ISCL showed superior performance comparable to a supervised

learning-based method, which is encouraging considering ISCL is an unpaired image denoising method. To the best of our knowledge, it is the first cooperative learning approach wherein CycleGAN and a self-residual learning-based network can complement each other under novel constraints (e.g., bypass-consistency, discriminator boosting, and noise-consistency). We discovered that the cooperative learning helps to converge faster to the optimal point than vanilla CycleGAN. Moreover, ISCL can arrive at better optimal point even though the network architecture is same as that of CycleGAN. As per our assumption in III, we demonstrated that our proposed constraints can reduce the mapping space of prediction of CycleGAN, so that the results are closed to ground-truth. We conclude that ISCL can be applied to the real-world examples such as in the medical domain that includes complex heterogeneous noise. In the future, we plan to explore other image restoration applications of ISCL, such as single image super-resolution.

REFERENCES

- [1] K. Dabov, A. Foi, V. Katkovnik, and K. Egiazarian, "Image denoising by sparse 3-d transform-domain collaborative filtering," *IEEE Trans. Image Process.*, vol. 16, no. 8, pp. 2080–2095, Aug. 2007.
- [2] J. Batson and L. Royer, "Noise2Self: Blind denoising by self-supervision," in *Proc. Int. Conf. Mach. Learn.*, Mar. 2019, pp. 524–533.
- [3] K. Zhang, W. Zuo, Y. Chen, D. Meng, and L. Zhang, "Beyond a gaussian denoiser: Residual learning of deep cnn for image denoising," *IEEE Trans. Image Process.*, vol. 26, no. 7, pp. 3142–3155, Jul. 2017.
- [4] T. Minh Quan, D. Grant Colburn Hildebrand, K. Lee, L. A. Thomas, A. T. Kuan, W.-C. Allen Lee, and W.-K. Jeong, "Removing imaging artifacts in electron microscopy using an asymmetrically cyclic adversarial network without paired training data," in *Proc. IEEE Int. Conf. Comput. Vis. Workshop*, Oct. 2019.
- [5] Z. Hong, X. Fan, T. Jiang, and J. Feng, "End-to-end unpaired image denoising with conditional adversarial networks," in *Proc. Assoc. Adv. Artif. Intell.*, Apr. 2020, pp. 4140–4149.
- [6] A. Buades, B. Coll, and J.-M. Morel, "A non-local algorithm for image denoising," in *Proc. IEEE Comput. Soc. Conf. Comput. Vis. Pattern Recognit.*, vol. 2, Jun. 2005, pp. 60–65.
- [7] J. Mairal, F. Bach, J. Ponce, G. Sapiro, and A. Zisserman, "Non-local sparse models for image restoration," in *Proc. IEEE Int. Conf. Comput. Vis.*, Sep. 2009, pp. 2272–2279.
- [8] C. Bao, J.-F. Cai, and H. Ji, "Fast sparsity-based orthogonal dictionary learning for image restoration," in *Proc. IEEE Int. Conf. Comput. Vis.*, Dec. 2013, pp. 3384–3391.
- [9] C. Bao, H. Ji, Y. Quan, and Z. Shen, "Dictionary learning for sparse coding: Algorithms and convergence analysis," *IEEE Trans. Pattern Anal. Mach. Intell.*, vol. 38, no. 7, pp. 1356–1369, Jul. 2016.
- [10] M. Elad and M. Aharon, "Image denoising via sparse and redundant representations over learned dictionaries," *IEEE Trans. Image Process.*, vol. 15, no. 12, pp. 3736–3745, Dec. 2006.
- [11] V. Pappas, Y. Romano, J. Sulam, and M. Elad, "Convolutional dictionary learning via local processing," in *Proc. IEEE Int. Conf. Comput. Vis.*, Oct. 2017, pp. 5296–5304.
- [12] C. R. Vogel and M. E. Oman, "Iterative methods for total variation minimization," *SIAM J. Sci. Comput.*, vol. 17, no. 1, pp. 227–238, Jan. 1996.
- [13] L. A. Vese and S. J. Osher, "Image denoising and decomposition with total variation minimization and oscillatory functions," *J. Math. Imaging Vis.*, vol. 20, no. 1-2, pp. 7–18, Jan. 2004.
- [14] P. Getreuer, "Rudin-Osher-Fatemi total variation denoising using split bregman," *Image Process. On Line*, vol. 2, pp. 74–95, 2012.
- [15] S. Lefkimmiatis, "Universal denoising networks: a novel cnn architecture for image denoising," in *Proc. IEEE conf. Comput. Vis. Pattern Recognit.*, Jun. 2018, pp. 3204–3213.
- [16] A. Krull, T.-O. Buchholz, and F. Jug, "Noise2void-learning denoising from single noisy images," in *Proc. IEEE conf. Comput. Vis. Pattern Recognit.*, Jun. 2019, pp. 2129–2137.

- [17] Y. Quan, M. Chen, T. Pang, and H. Ji, "Self2Self with dropout: Learning self-supervised denoising from single image," in *Proc. IEEE conf. Comput. Vis. Pattern Recognit.*, Jun. 2020, pp. 1890–1898.
- [18] D. G. C. Hildebrand, B. J. Graham, and W.-C. A. Lee, "Gridtape for fast nanoscale imaging," 2017.
- [19] B. J. Graham, D. G. C. Hildebrand, and W.-C. A. Lee, "Gridtape imaging stage," 2018.
- [20] B. J. Graham, D. G. C. Hildebrand, A. T. Kuan, J. T. Maniates-Selvin, L. A. Thomas, B. L. Shanny, and W.-C. A. Lee, "High-throughput transmission electron microscopy with automated serial sectioning," *bioRxiv*, 2019. [Online]. Available: <https://www.biorxiv.org/content/early/2019/06/02/657346>
- [21] J.-Y. Zhu, T. Park, P. Isola, and A. A. Efros, "Unpaired image-to-image translation using cycle-consistent adversarial networks," in *Proc. IEEE Int. Conf. Comput. Vis.*, 2017, pp. 2223–2232.
- [22] V. Jain and S. Seung, "Natural image denoising with convolutional networks," *Proc. Adv. Neural Inf. Process. Syst.*, vol. 21, pp. 769–776, 2008.
- [23] H. C. Burger, C. J. Schuler, and S. Harmeling, "Image denoising: Can plain neural networks compete with bm3d?" in *Proc. IEEE conf. Comput. Vis. Pattern Recognit.* IEEE, 2012, pp. 2392–2399.
- [24] X. Mao, C. Shen, and Y.-B. Yang, "Image restoration using very deep convolutional encoder-decoder networks with symmetric skip connections," in *Proc. Adv. Neural Inf. Process. Syst.*, D. D. Lee, M. Sugiyama, U. V. Luxburg, I. Guyon, and R. Garnett, Eds., 2016, pp. 2802–2810.
- [25] S. Lefkimmiatis, "Non-local color image denoising with convolutional neural networks," in *Proc. IEEE conf. Comput. Vis. Pattern Recognit.*, Jul. 2017, pp. 3587–3596.
- [26] K. He, X. Zhang, S. Ren, and J. Sun, "Deep residual learning for image recognition," in *Proc. IEEE conf. Comput. Vis. Pattern Recognit.*, 2016, pp. 770–778.
- [27] S. Ioffe and C. Szegedy, "Batch normalization: Accelerating deep network training by reducing internal covariate shift," ser. *Proc. Int. Conf. Mach. Learn.*, F. Bach and D. Blei, Eds., vol. 37, Lille, France, Jul. 2015, pp. 448–456.
- [28] J. Lehtinen, J. Munkberg, J. Hasselgren, S. Laine, T. Karras, M. Aittala, and T. Aila, "Noise2Noise: Learning image restoration without clean data," in *Proc. Int. Conf. Mach. Learn.*, J. Dy and A. Krause, Eds., vol. 80, Jul. 2018, pp. 2965–2974.
- [29] D. Ulyanov, A. Vedaldi, and V. Lempitsky, "Deep image prior," in *Proc. IEEE conf. Comput. Vis. Pattern Recognit.*, Jun. 2018, pp. 9446–9454.
- [30] J. Chen, J. Chen, H. Chao, and M. Yang, "Image blind denoising with generative adversarial network based noise modeling," in *Proc. IEEE conf. Comput. Vis. Pattern Recognit.*, 2018, pp. 3155–3164.
- [31] H. S. Park, J. Baek, S. K. You, J. K. Choi, and J. K. Seo, "Unpaired image denoising using a generative adversarial network in x-ray ct," *IEEE Access*, vol. 7, pp. 110414–110425, 2019.
- [32] X. Wu, M. Liu, Y. Cao, D. Ren, and W. Zuo, "Unpaired learning of deep image denoising," in *Eur. Conf. Comput. Vis.* Springer, 2020, pp. 352–368.
- [33] I. Goodfellow, J. Pouget-Abadie, M. Mirza, B. Xu, D. Warde-Farley, S. Ozair, A. Courville, and Y. Bengio, "Generative adversarial nets," in *Proc. Adv. Neural Inf. Process. Syst.*, 2014, pp. 2672–2680.
- [34] I. Gulrajani, F. Ahmed, M. Arjovsky, V. Dumoulin, and A. C. Courville, "Improved training of wasserstein gans," in *Proc. Adv. Neural Inf. Process. Syst.*, 2017, pp. 5767–5777.
- [35] M. Arjovsky, S. Chintala, and L. Bottou, "Wasserstein generative adversarial networks," in *Proc. Int. Conf. Mach. Learn.*, vol. 70, Aug. 2017, pp. 214–223.
- [36] J. H. Lim and J. C. Ye, "Geometric gan," [Online]. Available: <https://arxiv.org/abs/1705.02894>
- [37] B. Han, Q. Yao, X. Yu, G. Niu, M. Xu, W. Hu, I. Tsang, and M. Sugiyama, "Co-teaching: Robust training of deep neural networks with extremely noisy labels," in *Advances in neural information processing systems*, 2018, pp. 8527–8537.
- [38] P. Izmailov, D. Podoprikin, T. Garipov, D. Vetrov, and A. G. Wilson, "Averaging weights leads to wider optima and better generalization," *Assoc. Uncertainty Artif. Intell.*, 2018.
- [39] M. Zhang, J. Lucas, J. Ba, and G. E. Hinton, "Lookahead optimizer: k steps forward, 1 step back," in *Proc. Adv. Neural Inf. Process. Syst.*, Dec. 2019, pp. 9597–9608.
- [40] L. Liu, H. Jiang, P. He, W. Chen, X. Liu, J. Gao, and J. Han, "On the variance of the adaptive learning rate and beyond," *Proc. Int. Conf. Learn. Represent.*, 2020.
- [41] "Low dose ct grand challenge," 2016. [Online]. Available: <https://www.aapm.org/grandchallenge/>
- [42] H. Nam and H.-E. Kim, "Batch-instance normalization for adaptively style-invariant neural networks," in *Proc. Adv. Neural Inf. Process. Syst.*, vol. 31, 2018, pp. 2558–2567.
- [43] D. Ulyanov, A. Vedaldi, and V. Lempitsky, "Instance normalization: The missing ingredient for fast stylization," [Online]. Available: <https://arxiv.org/abs/1607.08022>
- [44] J. Long, E. Shelhamer, and T. Darrell, "Fully convolutional networks for semantic segmentation," in *Proc. IEEE conf. Comput. Vis. Pattern Recognit.*, 2015, pp. 3431–3440.